Title: Entanglement maximization and dynamics via joint continuous measurement

Date: Jun 06, 2016 03:30 PM

URL: http://pirsa.org/16060089

Abstract: We investigate the quantum trajectories of jointly monitored transmon qubits, tracking measurement-induced entanglement creation as a continuous process. The quantum trajectories naturally split into low and high entanglement classes corresponding to partial parity collapse. We theoretically calculate the distribution of concurrence at any given time and show good agreement with the constructed histogram of measured concurrence trajectories. The distribution exhibits a sharp cut-off in the high concurrence limit, defining a maximal concurrence boundary. The most probable paths of the two classes, starting in a separable state and ending in either an entangled state or separable state, are found and compared with the experimentally constructed paths of the sub-ensemble. The most likely time for the transmon qubits to reach their highest concurrence can also be extracted from the most likely path analysis.

Quantum trajectories and their statistics for remotely entangled quantum bits

Areeya Chantasri,[1,2] Mollie E. Kimchi-Schwartz,[3] Nicolas Roch,[4] Irfan Siddiqi,[3] and Andrew N. Jordan[1,2,5]

[1] *Department of Physics and Astronomy, University of Rochester, Rochester, NY 14627, USA*
[2] *Center for Coherence and Quantum Optics, University of Rochester, Rochester, NY 14627, USA*
[3] *Quantum Nanoelectronics Laboratory, Department of Physics, University of California, Berkeley, California 94720, USA*
[4] *Université Grenoble Alpes, Institut NEEL, F-38000 Grenoble, France and CNRS, Institut NEEL, F-38000 Grenoble, France*
[5] *Institute for Quantum Studies, Chapman University, 1 University Drive, Orange, CA 92866, USA*

(Dated: May 19, 2016)

We experimentally and theoretically investigate the quantum trajectories of jointly monitored transmon qubits embedded in spatially separated microwave cavities. Using nearly quantum-noise limited superconducting amplifiers and an optimized setup to reduce signal loss between cavities, we can efficiently track measurement-induced entanglement generation as a continuous process for single realizations of the experiment. The quantum trajectories of transmon qubits naturally split into low and high entanglement classes. The distribution of concurrence is found at any given time and we explore the dynamics of entanglement creation in the state space. The distribution exhibits a sharp cut-off in the high concurrence limit, defining a maximal concurrence boundary. The most likely paths of the qubits' trajectories are also investigated, resulting in three probable paths, gradually projecting the system to two even subspaces and an odd subspace, conforming to a "half-parity" measurement. We also investigate the most likely time for the individual trajectories to reach their most entangled state, and find that there are two solutions for the local maximum, corresponding to the low and high entanglement routes. The theoretical predictions show excellent agreement with the experimental entangled qubit trajectory data.

I. INTRODUCTION

Measurement-induced entanglement of spatially separated quantum systems is a startling prediction of quantum mechanics [1–7]. Recent experiments have demonstrated include the observation of quantum states of light in resonators [19], as well as nearly quantum-limited parametric amplifiers [20, 21].

The improvement of coherent quantum hardware has brought with it a renewed focus on the physics of quan-

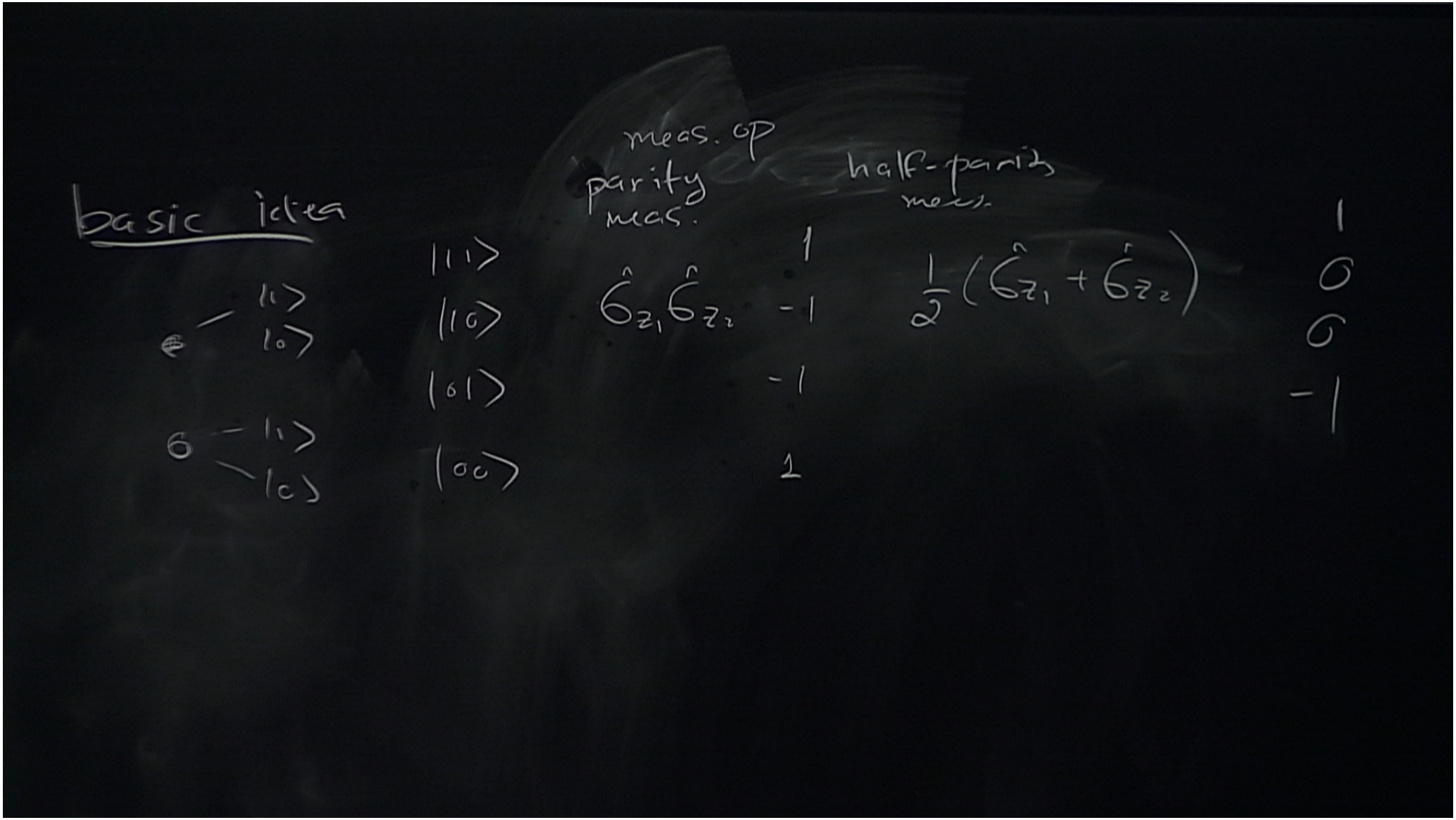
basic idea
meas. op
parity meas.
half-parity meas.
|11>
|10>
|01>
|00>
1
-1
-1
1
$\hat{\sigma}_{z_1}\hat{\sigma}_{z_2}$
$\frac{1}{2}(\hat{\sigma}_{z_1}+\hat{\sigma}_{z_2})$
1
0
0
-1
|1>
|0>
|1>
|0>

Example: Two qubits measured in σ_z basis

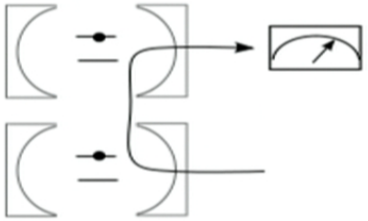

- Joint weak measurement of two qubits
- Measuring
  $\sigma_{z,1} + \sigma_{z,2} = -2\,(|00\rangle), 0\,(|01\rangle, |10\rangle), +2\,(|11\rangle)$
- No qubit rotation
- Entanglement creation due to the joint qubit measurement

Experiment: two superconducting qubits coupled to spatially separated microwave waveguide cavities [N. Roch, et.al., PRL, **112**, 170501, (2014)]

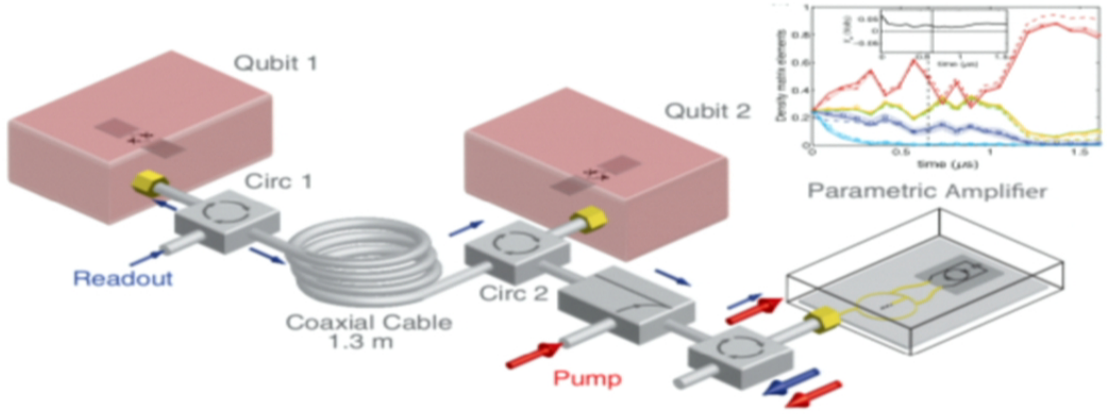

Example: Two qubits measured in σ_z basis

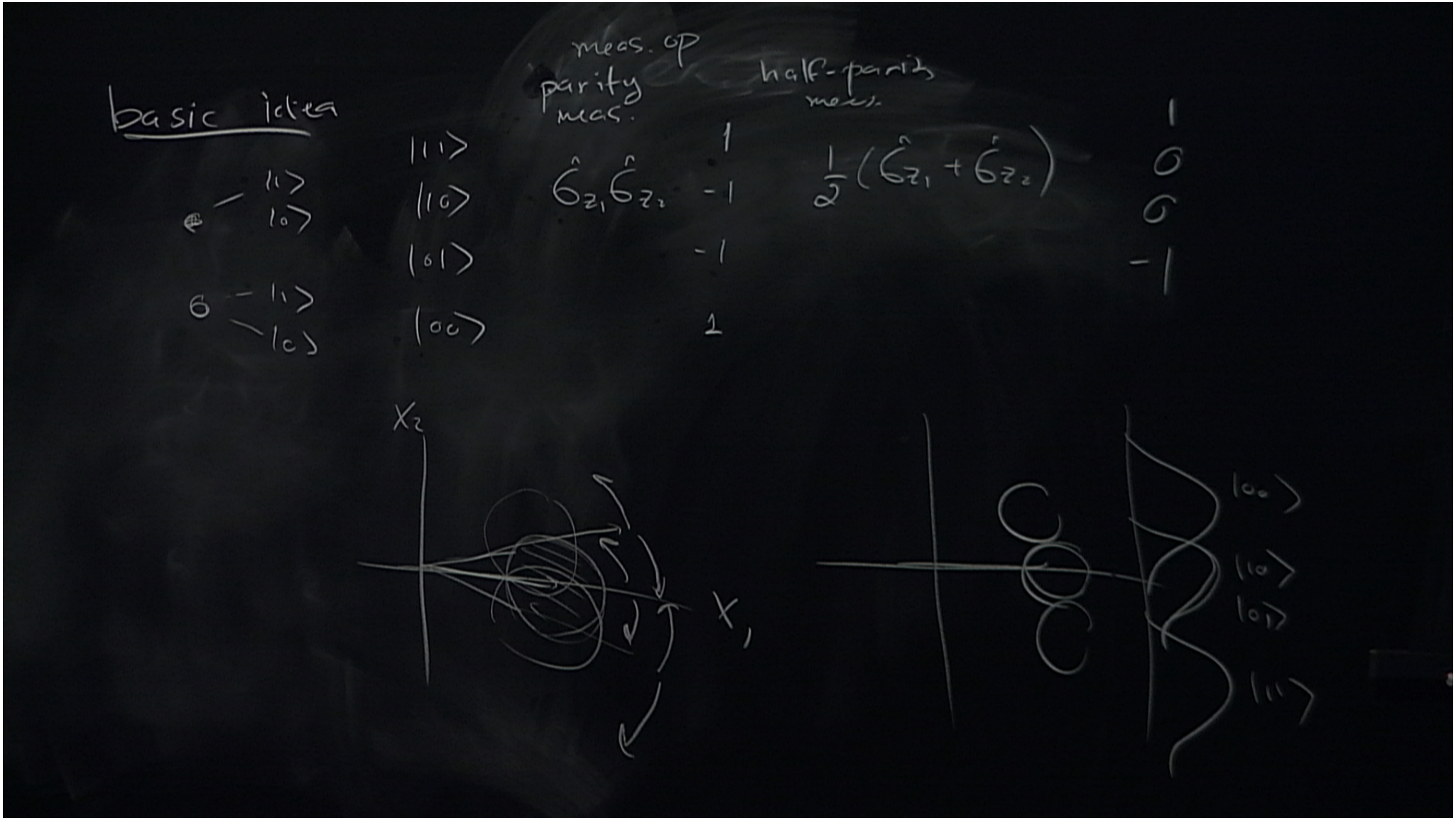
basic idea
meas. op
parity meas.
half-parity meas.
|11>
|10>
|01>
|00>
1
-1
-1
1
1
0
0
-1
X2
X1
|00>
|10>
|01>
|11>

output of the circulator is routed to a high-efficiency amplification chain (not shown). The upper inset represents the tribution of the microwave field in the (X_1, X_2) quadrature plane at the output of the amplifier. The three possible comes correspond to three different subspaces: $|00\rangle$, $|11\rangle$, and the odd-parity subspace (spanned by the $|01\rangle$ and $|10\rangle$ states). shows the evolution in time of the measurement outcome probability distribution $p(V_t)$. (c) shows the agreement between experimentally-generated conditional tomography $x_i(V_t)$ (symbols and shaded error bars) and the theoretical Bayesian onstruction (dashed lines), for a single time $t = 0.48\ \mu s$. In panel (d), we use such reconstructions to predict and verify the jectory of a single iteration of the experiment, showing both density matrix elements x_i and concurrence (inset).

n, we can engineer an entangling measurement with characteristic measurement time ranging from several ndred nanoseconds to several microseconds: critically, se timescales are easily resolvable experimentally. The namics or the trajectory of the system state can be ob- ned via the full master equations [46, 47], using a two- vity polaron transformation to account for the cavity gree of freedom, giving the stochastic master equation the qubit trajectories. Alternatively, in a limit of ge cavity decay rate $\kappa \gg |\chi|$, the qubits evolution can continuously tracked via the quantum Bayesian ap- oach [2, 3], inferring the current states of the system m the measurement readouts and how likely they are occur. The two approaches both show good agreement tracking the qubit pair state [12].

In this paper, we focus on the quantum Bayesian ap- oach, as it is directly related to the probability distri- tion of the measurement readout, and naturally leads the probability distribution of quantum trajectories. t us denote $p(V_t|i)$ as a probability density function a measurement readout V_t conditioned on the two- bit states i, where $i = 1, 2, 3, 4$ representing the states $\rangle, |01\rangle, |10\rangle, |11\rangle$ respectively. The quantum Bayesian date for this type of double-qubit measurement pro- readout V_t,

$$\rho_{ij}(t) = \frac{\rho_{ij}(0)\sqrt{p(V_t|i)p(V_t|j)}e^{-\gamma_{ij}t}}{\sum_{k=1}^{4}\rho_{kk}(0)p(V_t|k)}, \qquad (1)$$

where ρ_{ij} denotes the ij element of the two-qubit density matrix and γ_{ij} is a decoherence rate associated to the matrix element.

We define the readout $V_t \equiv (f/t)\int_0^t \tilde{V}(t')\mathrm{d}t' - v_0$ as a time-average of a raw homodyne voltage signal rescaled with a weight factor f and an off-set v_0, where f is chosen so that the variance $\sigma^2_{V_t} = 1/4\eta_m t$ is a function of a quantum efficiency of the homodyne measurement, $\eta_m \approx 0.22$. The total probability distribution $p(V_t) = \sum_{k=1}^{4}\rho_{kk}(0)p(V_t|k)$, shown in Figure 1(b), slowly resolves into the three peaks expected for a half-parity measurement.

The conditional readout distributions are well-approximated by Gaussian functions, giving $p(V_t|i) = (t/\pi s)^{-1/2}\exp\{-(V_t - \delta v_i)^2 t/s\}$ with the centering signals $\delta v_i = v_i - v_0$ for $i = 1, \ldots, 4$, where $s = 1/2\eta_m$. The measurement process cannot distinguish the two states in the odd-parity subspace, therefore the readout distributions corresponding to the states $|01\rangle$ and $|10\rangle$ are completely (or nearly) overlapped, giving $\delta v_2 \approx \delta v_3 \approx 0$ and

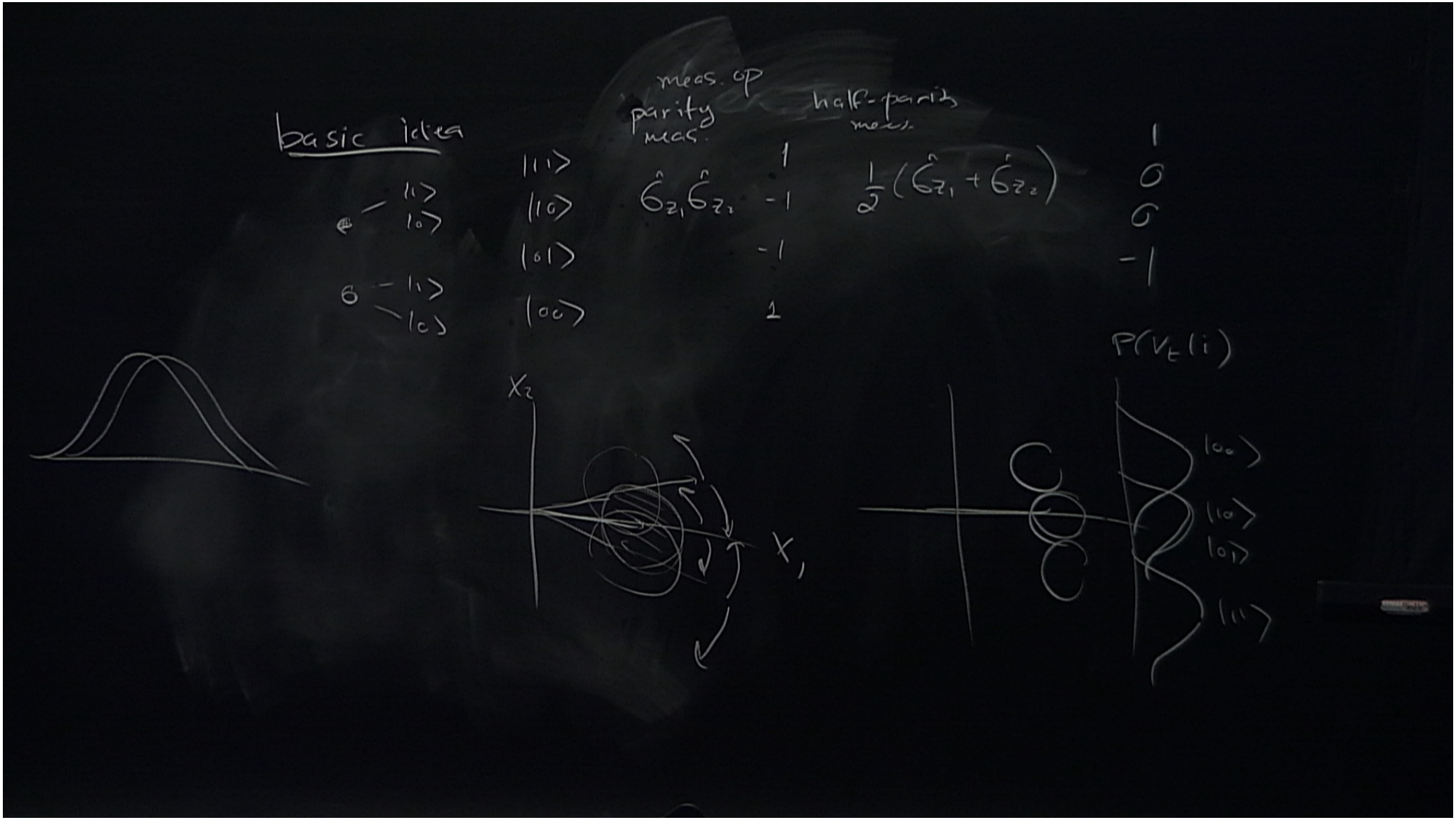
basic idea
meas. of parity meas.
half-parity meas.
|11>
|10>
|01>
|00>
1
-1
-1
1
$\hat{\sigma}_{z_1}\hat{\sigma}_{z_2}$
$\frac{1}{2}(\hat{\sigma}_{z_1}+\hat{\sigma}_{z_2})$
1
0
0
-1
X_2
X_1
$P(V_t(i))$
|00>
|10>
|01>
|11>

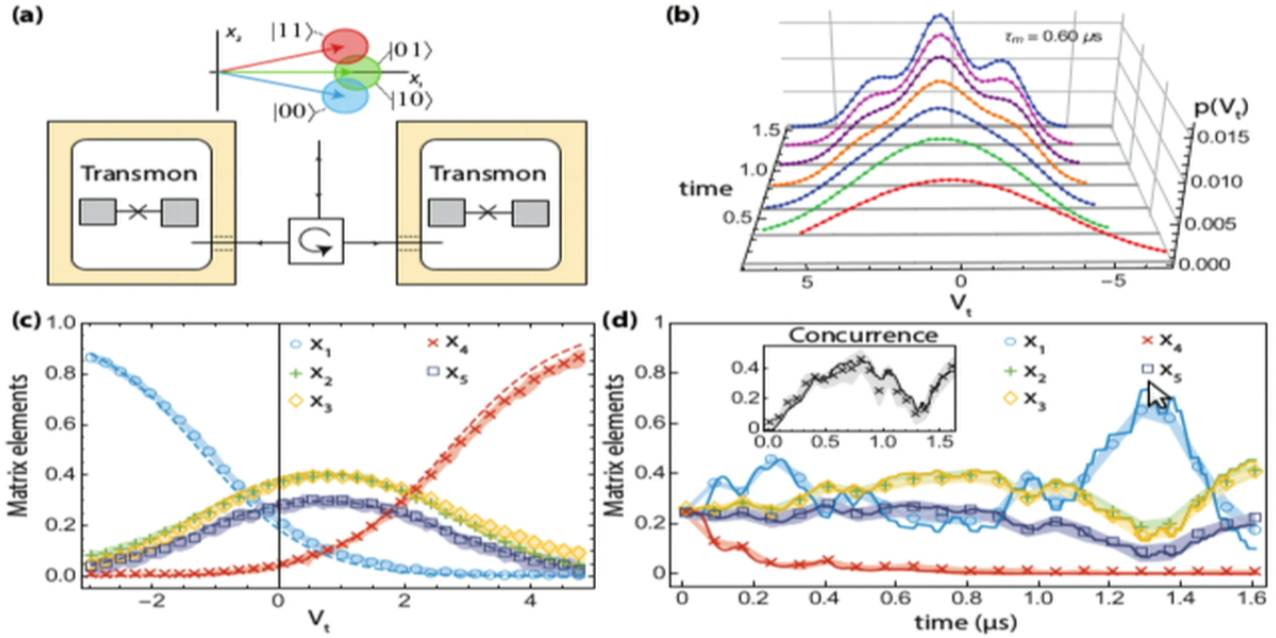

FIG. 1. (Color) Experimental setup and transmon qubits trajectories. (a) shows a simplified illustration of the experimental setup. Two Transmon qubits in two remote cavities are linked via a single microwave circulator in a *bounce-bounce* geometry; the output of the circulator is routed to a high-efficiency amplification chain (not shown). The upper inset represents the distribution of the microwave field in the (X_1, X_2) quadrature plane at the output of the amplifier. The three possible outcomes correspond to three different subspaces: $|00\rangle$, $|11\rangle$, and the odd-parity subspace (spanned by the $|01\rangle$ and $|10\rangle$ states). (b) shows the evolution in time of the measurement outcome probability distribution $p(V_t)$. (c) shows the agreement between the experimentally-generated conditional tomography $x_i(V_t)$ (symbols and shaded error bars) and the theoretical Bayesian reconstruction (dashed lines), for a single time $t = 0.48\ \mu s$. In panel (d), we use such reconstructions to predict and verify the trajectory of a single iteration of the experiment, showing both density matrix elements x_i and concurrence (inset).

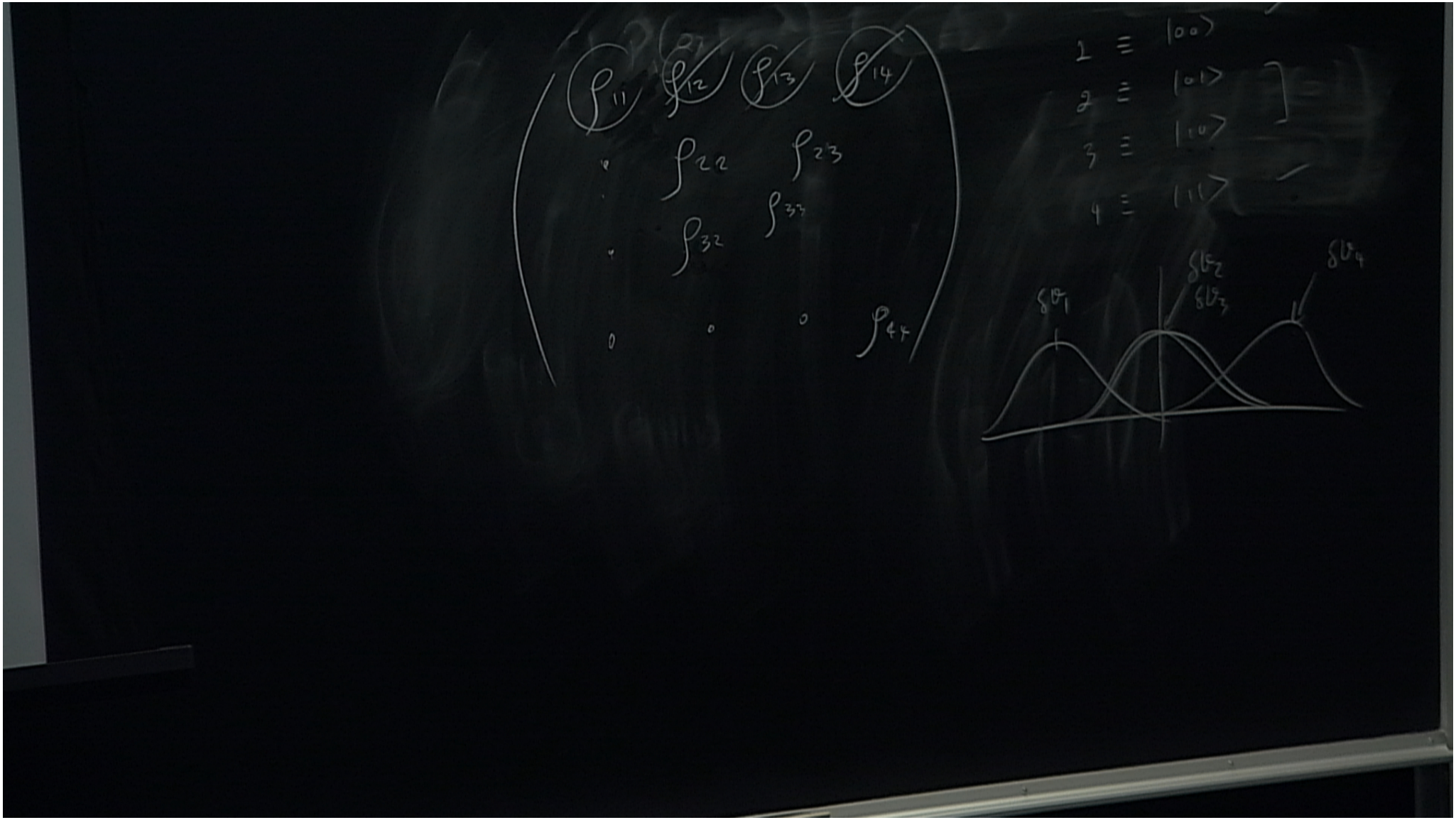
1 ≡ |00⟩
2 ≡ |01⟩
3 ≡ |10⟩
4 ≡ |11⟩

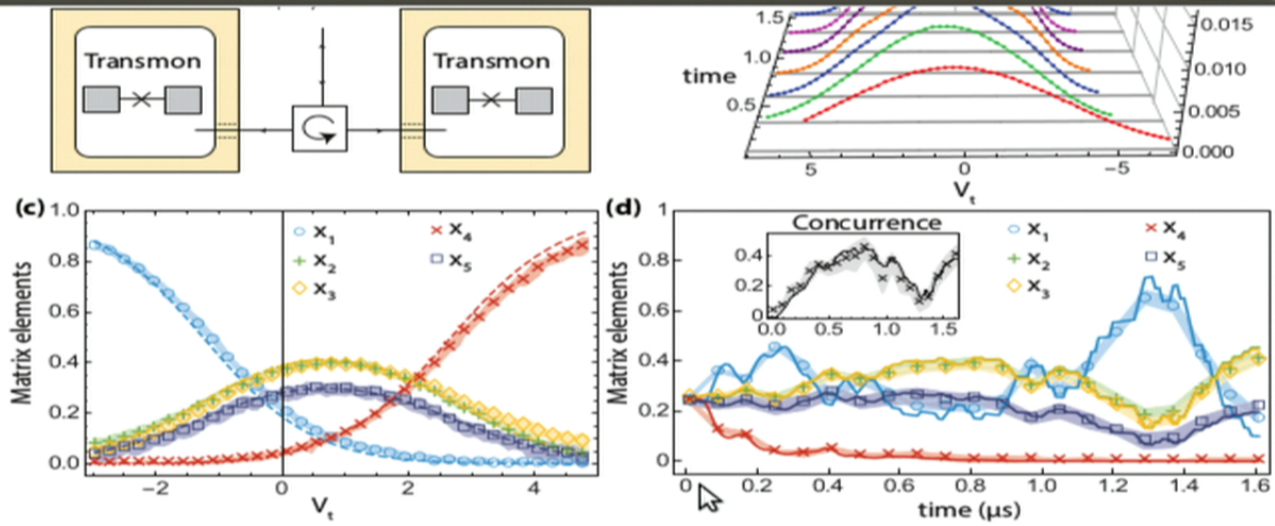

FIG. 1. (Color) Experimental setup and transmon qubits trajectories. (a) shows a simplified illustration of the experimer setup. Two Transmon qubits in two remote cavities are linked via a single microwave circulator in a *bounce-bounce* geome the output of the circulator is routed to a high-efficiency amplification chain (not shown). The upper inset represents distribution of the microwave field in the (X_1, X_2) quadrature plane at the output of the amplifier. The three poss outcomes correspond to three different subspaces: $|00\rangle$, $|11\rangle$, and the odd-parity subspace (spanned by the $|01\rangle$ and $|10\rangle$ stat (b) shows the evolution in time of the measurement outcome probability distribution $p(V_t)$. (c) shows the agreement betw the experimentally-generated conditional tomography $x_i(V_t)$ (symbols and shaded error bars) and the theoretical Baye reconstruction (dashed lines), for a single time $t = 0.48\ \mu s$. In panel (d), we use such reconstructions to predict and verify trajectory of a single iteration of the experiment, showing both density matrix elements x_i and concurrence (inset).

tem, we can engineer an entangling measurement with a characteristic measurement time ranging from several hundred nanoseconds to several microseconds: critically, these timescales are easily resolvable experimentally. The dynamics or the trajectory of the system state can be ob-

readout V_t,

$$\rho_{ij}(t) = \frac{\rho_{ij}(0)\sqrt{p(V_t|\,i)p(V_t|\,j)}e^{-\gamma_{ij}t}}{\sum_{k=1}^{4}\rho_{kk}(0)p(V_t|\,k)},$$

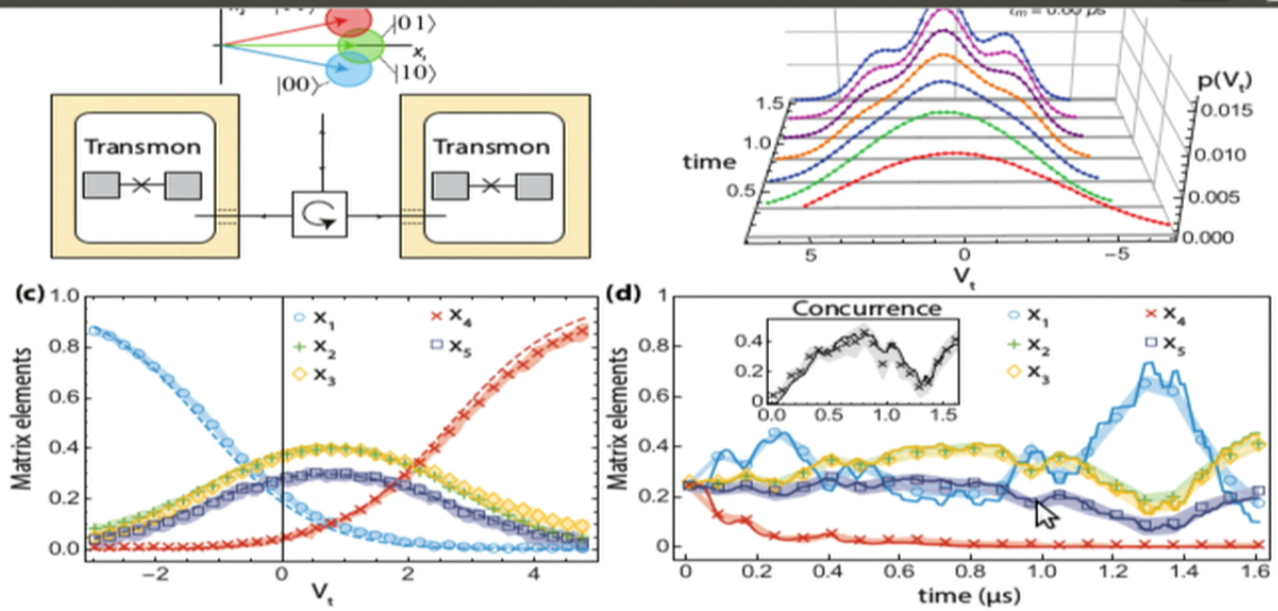

FIG. 1. (Color) Experimental setup and transmon qubits trajectories. (a) shows a simplified illustration of the experime setup. Two Transmon qubits in two remote cavities are linked via a single microwave circulator in a *bounce-bounce* geome the output of the circulator is routed to a high-efficiency amplification chain (not shown). The upper inset represents distribution of the microwave field in the (X_1, X_2) quadrature plane at the output of the amplifier. The three poss outcomes correspond to three different subspaces: $|00\rangle$, $|11\rangle$, and the odd-parity subspace (spanned by the $|01\rangle$ and $|10\rangle$ stat (b) shows the evolution in time of the measurement outcome probability distribution $p(V_t)$. (c) shows the agreement betw the experimentally-generated conditional tomography $x_i(V_t)$ (symbols and shaded error bars) and the theoretical Baye reconstruction (dashed lines), for a single time $t = 0.48\ \mu s$. In panel (d), we use such reconstructions to predict and verify trajectory of a single iteration of the experiment, showing both density matrix elements x_i and concurrence (inset).

tem, we can engineer an entangling measurement with a characteristic measurement time ranging from several

readout V_t,

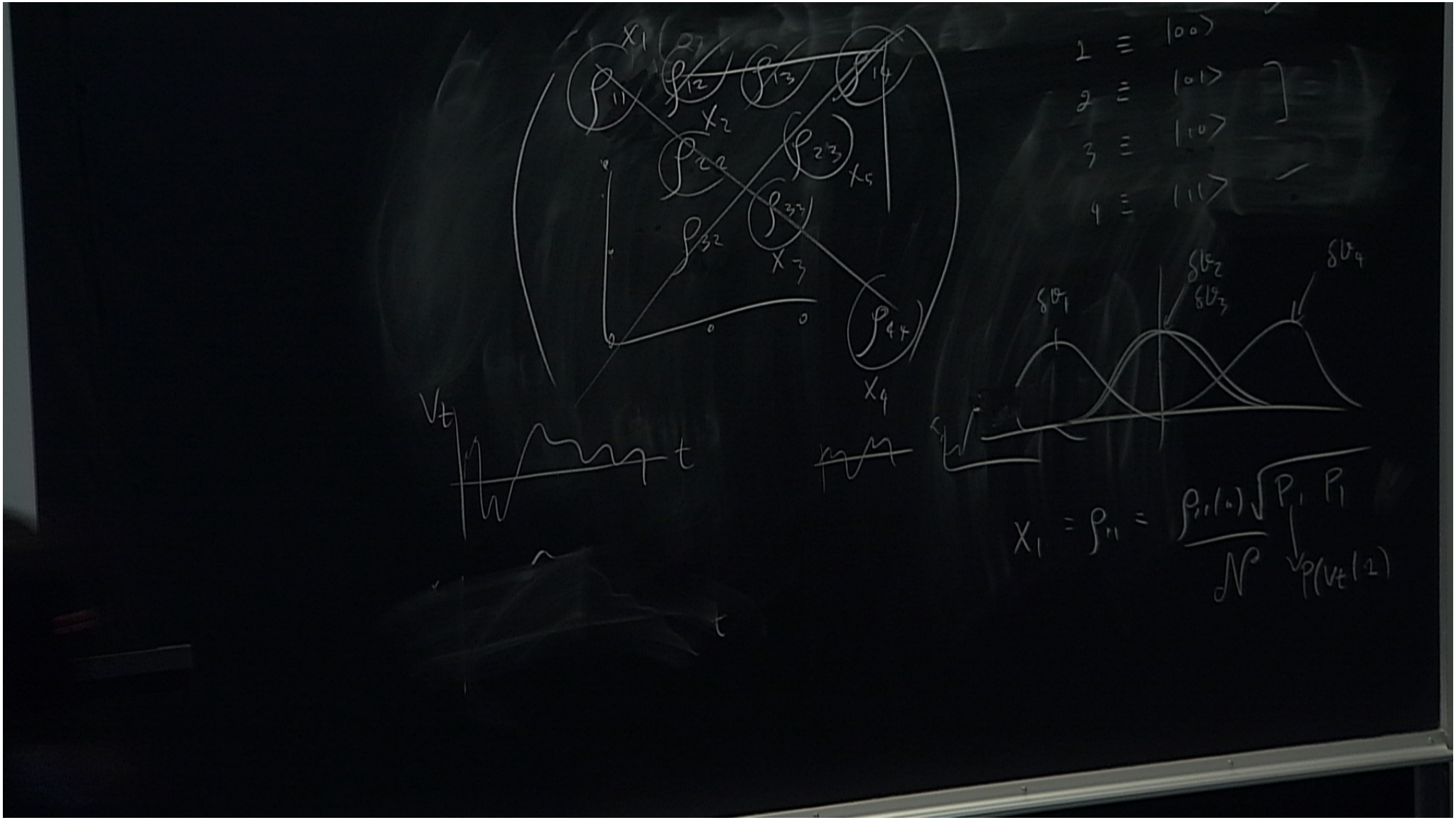
1 ≡ |00⟩
2 ≡ |01⟩
3 ≡ |10⟩
4 ≡ |11⟩
$X_1 = \rho_{11} = \frac{\rho_{1,(1,1)}\sqrt{P_1 P_1}}{N}$
V_t
t

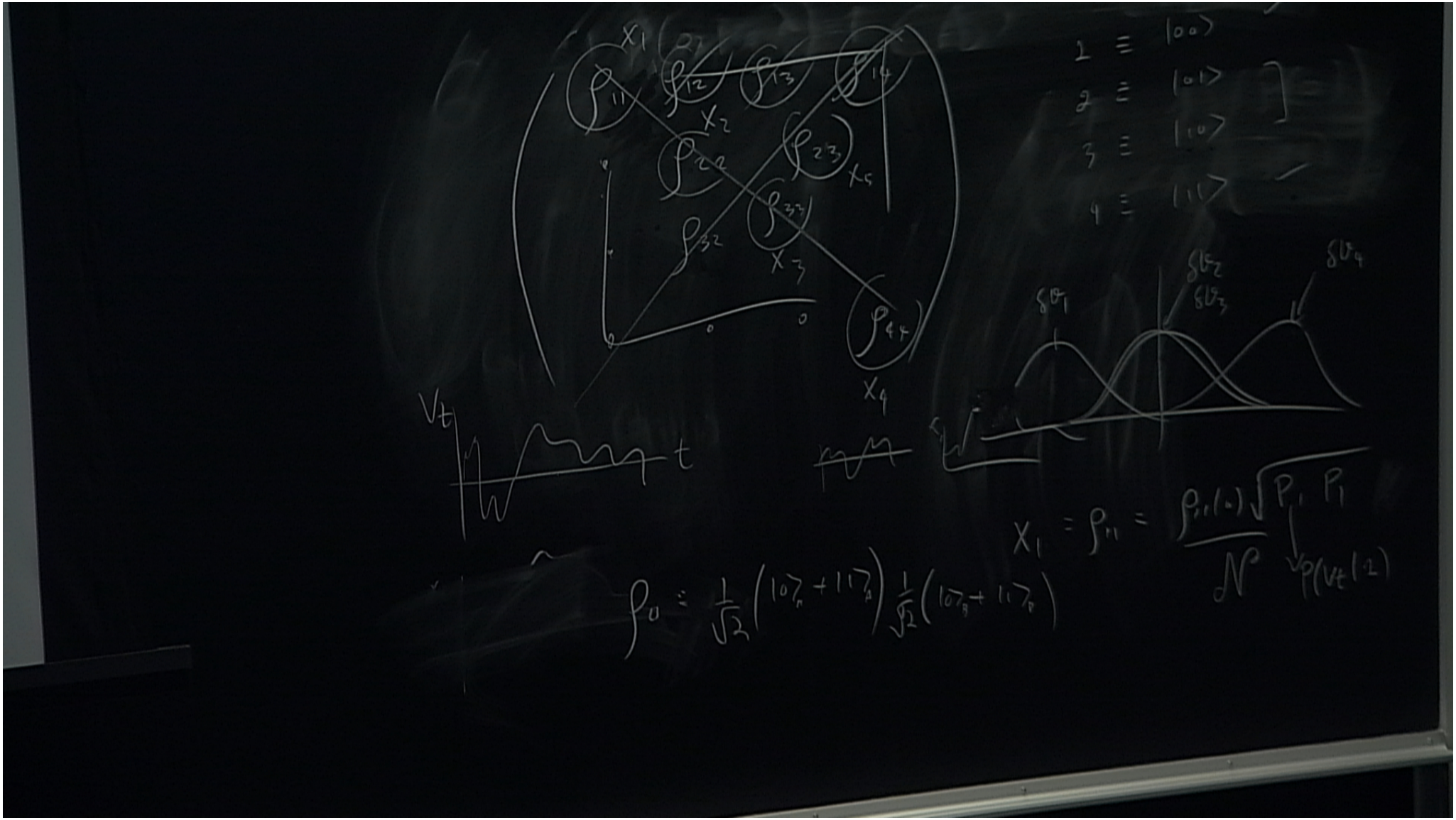
1 ≡ |00⟩
2 ≡ |01⟩
3 ≡ |10⟩
4 ≡ |11⟩
X1
X2
X3
X4
Vt
t
δθ1
δθ2
δθ3
δθ4
ρ0 = 1/√2 (|0⟩A + |1⟩A) 1/√2 (|0⟩B + |1⟩B)
Xi = ρii = ρi,(i-1) √(Pi Pi) / N
P(Vt|i)

the problem, Eq. (1). Consequently, the concurrence is controlled by V_t, as in Eq. (5). As can be seen from the inset of Figure 2(a), the concurrence, plotted as a function of the measured signal V_t is bounded from above for any fixed time t by some amount we call $\mathcal{C}_{\max}$, and consequently, any value of concurrence higher than that maximum (whose value will change as the time increases) cannot be realized. Therefore the probability distribution of concurrence has a sharp upper cut-off given by $\mathcal{C}_{\max}(t)$. Physically, this indicates that there is an upper limit on how fast entanglement can be created by the continuous measurement in this situation, even for rare events of the measurement process.

For the perfectly symmetric case in Eq. (5), we can find an analytic solution for the upper bound of the concurrence, knowing that $\cosh(x)$ has its minimum at $x = 0$, $\mathcal{C}_{\mathrm{ps},\hat{x}}(V_t)$ has its maximum at $V_t = 0$, so consequently, the concurrence upper bound is given by

$$\mathcal{C}_{\max,\mathrm{ps},\hat{x}}(t) = \frac{e^{-\gamma t} - e^{-\delta v^2 t/s}}{1 + e^{-\delta v^2 t/s}}. \tag{8}$$

The behaviour of this bound is a result of two competing rates, between the extra dephasing rate γ and a measurement rate $\delta v^2/s$. Eq. (8) increases from zero for small time and decays for long time after reaching its maximum concurrence as seen in Figure 2. The maximum possible concurrence for this qubit half-parity measurement and the time this happens can be obtained from this relation. More about the time to reach maximum concurrence will be discussed in Section IV C.

IV. MOST LIKELY PATH ANALYSIS

fine, $v_t = (f/\delta t)\int_t^{t+\delta t} V(t')\mathrm{d}t' - v_0$, as an instantane readout at time t with an integration time δt. Since readout v_t's are assumed Markovian and only depend the qubit states right before the measurement, a j probability density function for the readout realizatio given by,

$$\mathcal{P}(\{v_t\}) = \prod_{t'=0}^{t}\left\{\sum_{k=1}^{4} x_{k,t'}\, p(v_{t'}|k)\right\},$$

a product of probability distributions of $v_{t'}$ from t' to $t' = t$ with a time step δt. The probability fu tion for an instantaneous readout is given by $p(v_t|k$ $\sqrt{\delta t/\pi s}\,\exp\{-(v_t - \delta v_i)^2\delta t/s\}$ for $i = 1, 2, 3, 4$.

To derive the most likely path for these two-qubit jectories, we use the Bayesian update equation for two-qubit state Eq. (1), adapted to a state update ev time step δt, and then we maximize the joint proba ity density Eq. (9) constraining the state update eq tions. Following the most likely path analysis for qu tum states under continuous measurement [36, 37] introducing Lagrange multipliers $\{p_1, p_2, p_3, p_4, p_5\}$ the contraints, we obtain differential equations for an timal path in the qubits state space,

$$\partial_t x_i = +\frac{x_i}{s}\sum_{k=1}^{4} x_k\{2v_t(\delta v_i - \delta v_k) - \delta v_i^2 + \delta v_k^2\}, \tag{1}$$

$$\partial_t x_5 = -\gamma x_5 + \frac{x_5}{s}\left\{v_t(\delta v_2 + \delta v_3) - \frac{(\delta v_2^2 + \delta v_3^3)}{2} + \sum_{k=1}^{4} x_k(\delta v_k^2 - 2v_t\delta v_k)\right\}, \tag{1}$$

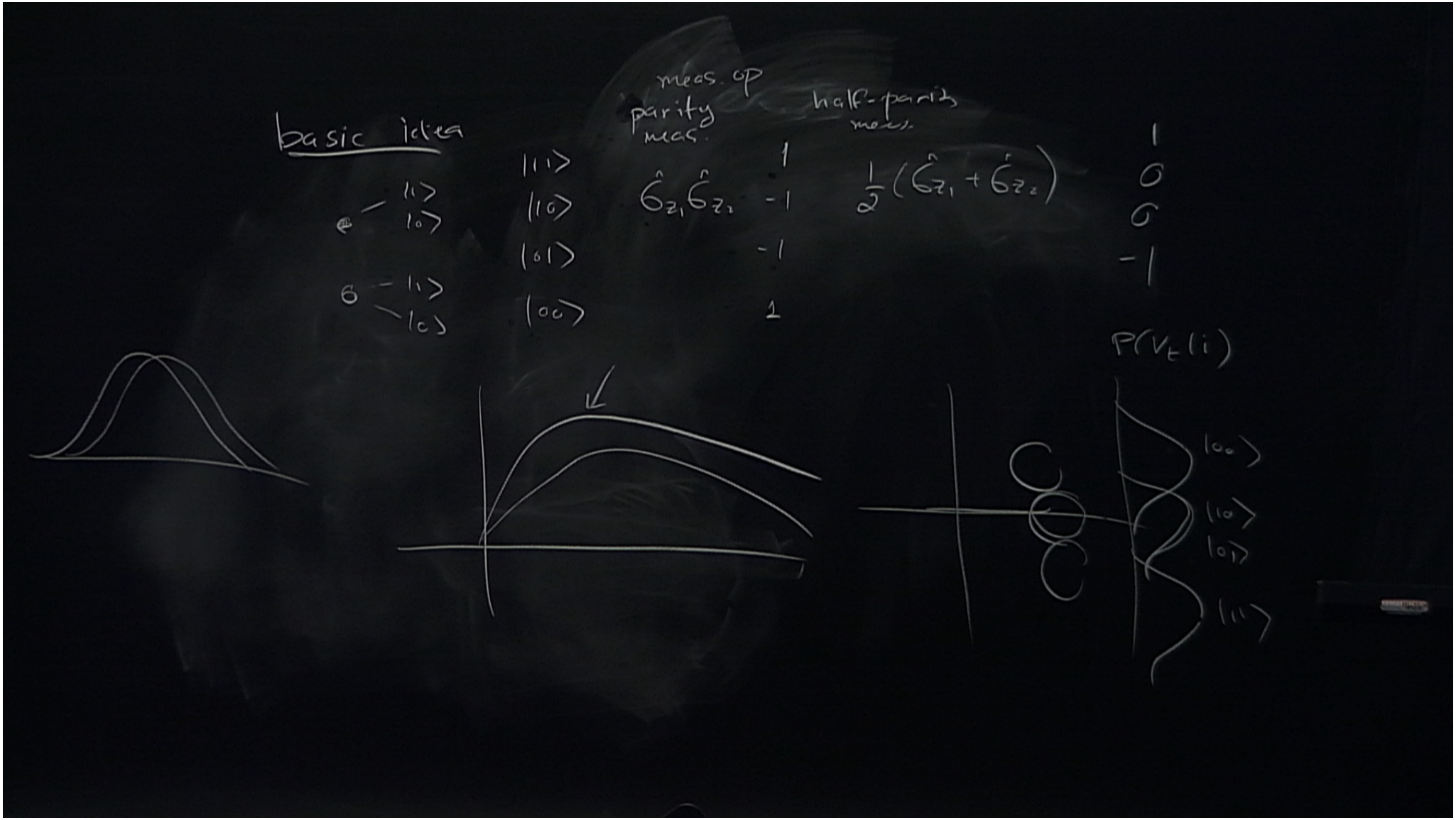
basic idea
meas. of parity meas.
half-parity meas.
|11>
|10>
|01>
|00>
$\hat{\sigma}_{z_1}\hat{\sigma}_{z_2}$
1
-1
-1
1
$\frac{1}{2}(\hat{\sigma}_{z_1}+\hat{\sigma}_{z_2})$
1
0
0
-1
$P(V_t(i))$
|00>
|10>
|01>
|11>

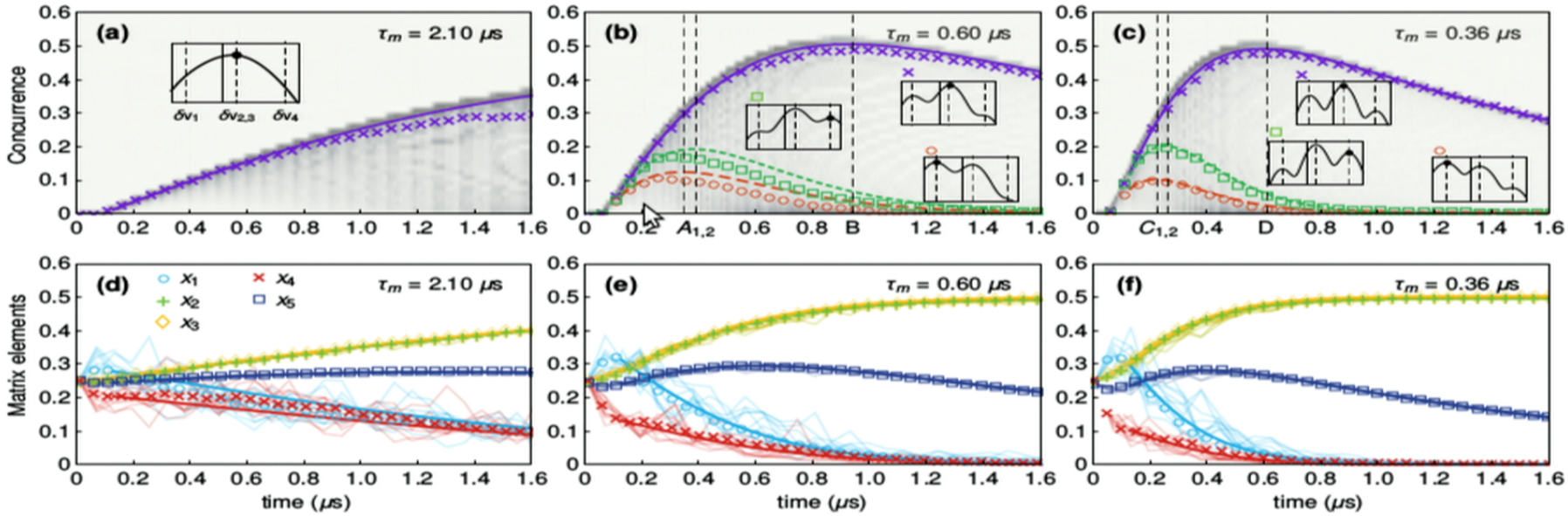

FIG. 3. (Color) The most likely paths from the theoretical prediction and the experimental data. The first, second, and third columns are from three different data sets, measuring the same qubits and cavities with three different measurement

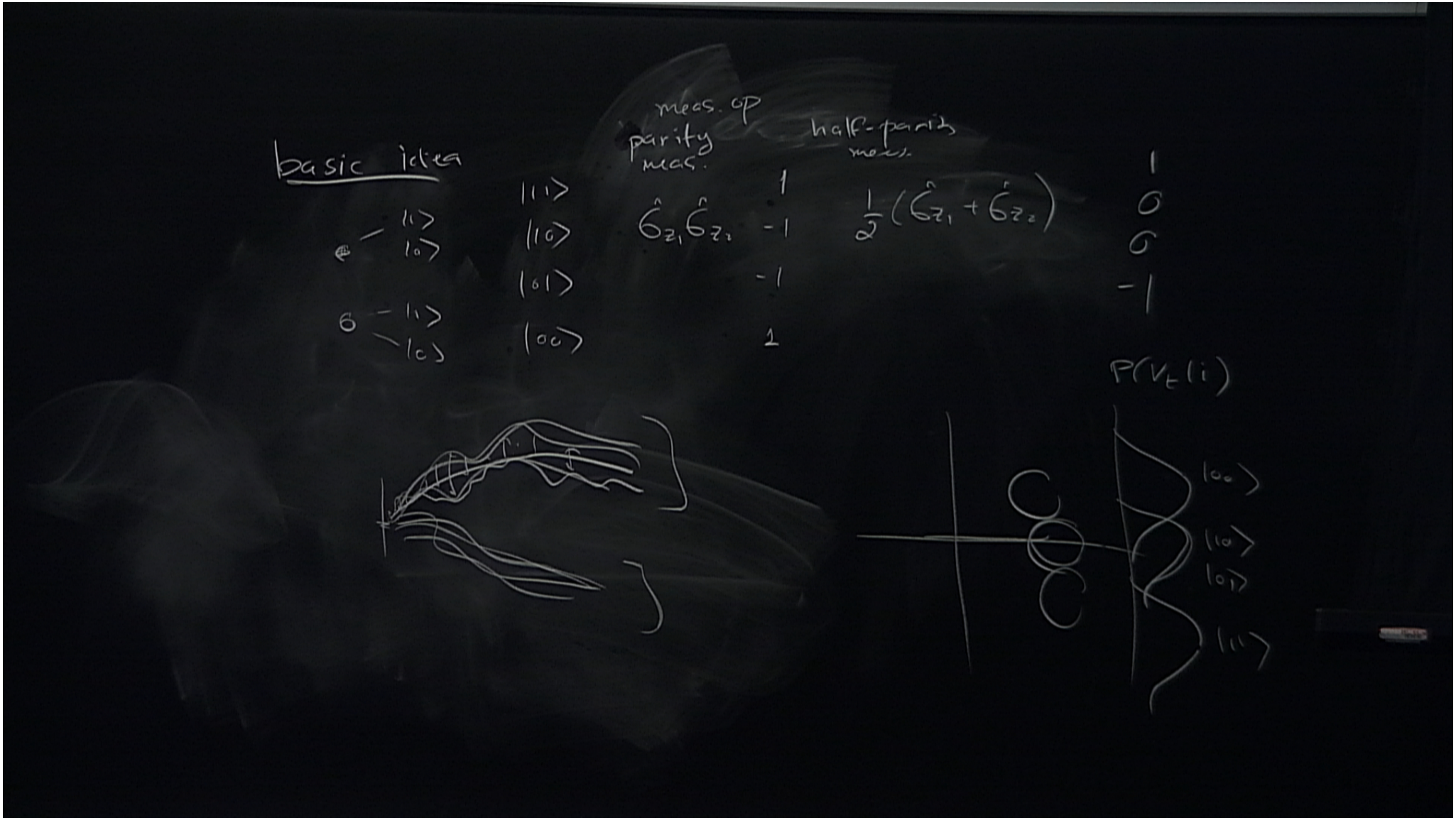
basic idea
meas. of parity meas.
half-parity meas.
|11>
|10>
|01>
|00>
1
-1
-1
1
1
0
0
-1
P(V_t(i)
|00>
|10>
|01>
|11>

corresponding to two branches of most likely paths collapsed to $|00\rangle$ and $|11\rangle$ states (low-concurrence branches), respectively. We note that this technique of finding multiple most likely paths is not under final-state constraints

surement strength using the initial state $\{x_1^0, ..., x_5^0\} = \{1/4, ..., 1/4\}$ would be good enough to compare with the experimental data. However, in the experiment, after the initial state has been prepared, the cavities take some time to reach their steady state condition, making the parameters $\delta v_1, ..., \delta v_4$ unstable during the first $\sim 0.13\mu s$ time. Therefore, we need to let the initial qubit state evolve and then find new "initial" states at time $t = 0.13\mu s$ for the theoretical most likely path calculation. We use the experimental most likely states at $t = 0.13\mu s$ (one for each branch) as the initial states in calculating the log-likelihood functions (the insets), which then lead to an excellent prediction of the most likely paths and their concurrence for the rest of the evolution.

We also note that the unequal two low-concurrence branches in Figure 3(b,c) happen because the population of the states drifts more toward the ground state $|00\rangle$ during the transient time, as a result of the qubit relaxation

the concurrence of the experimental most likely paths a
data points.

Ideally, the theoretical most likely paths predicte
from the log-likelihood Eq. (11) for each set of mea

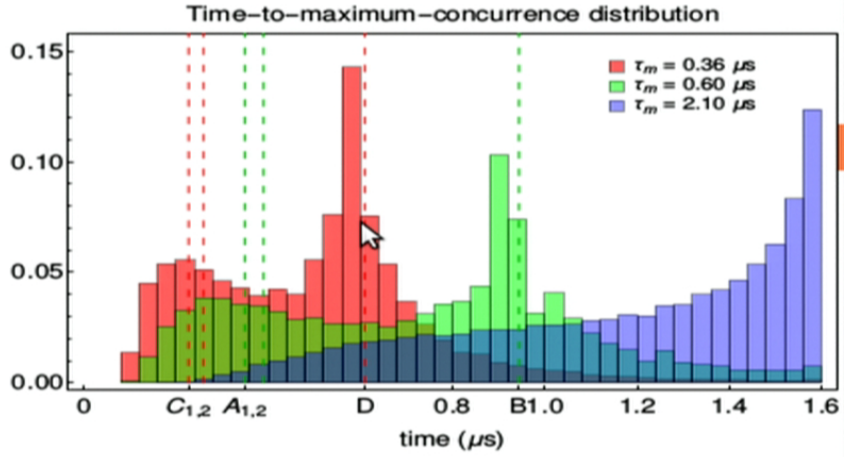

FIG. 4. (Color) Histograms of the time-to-maximum co
currence for individual trajectories for three measuremer
strengths indicated by the values of τ_m. For the two cases wit

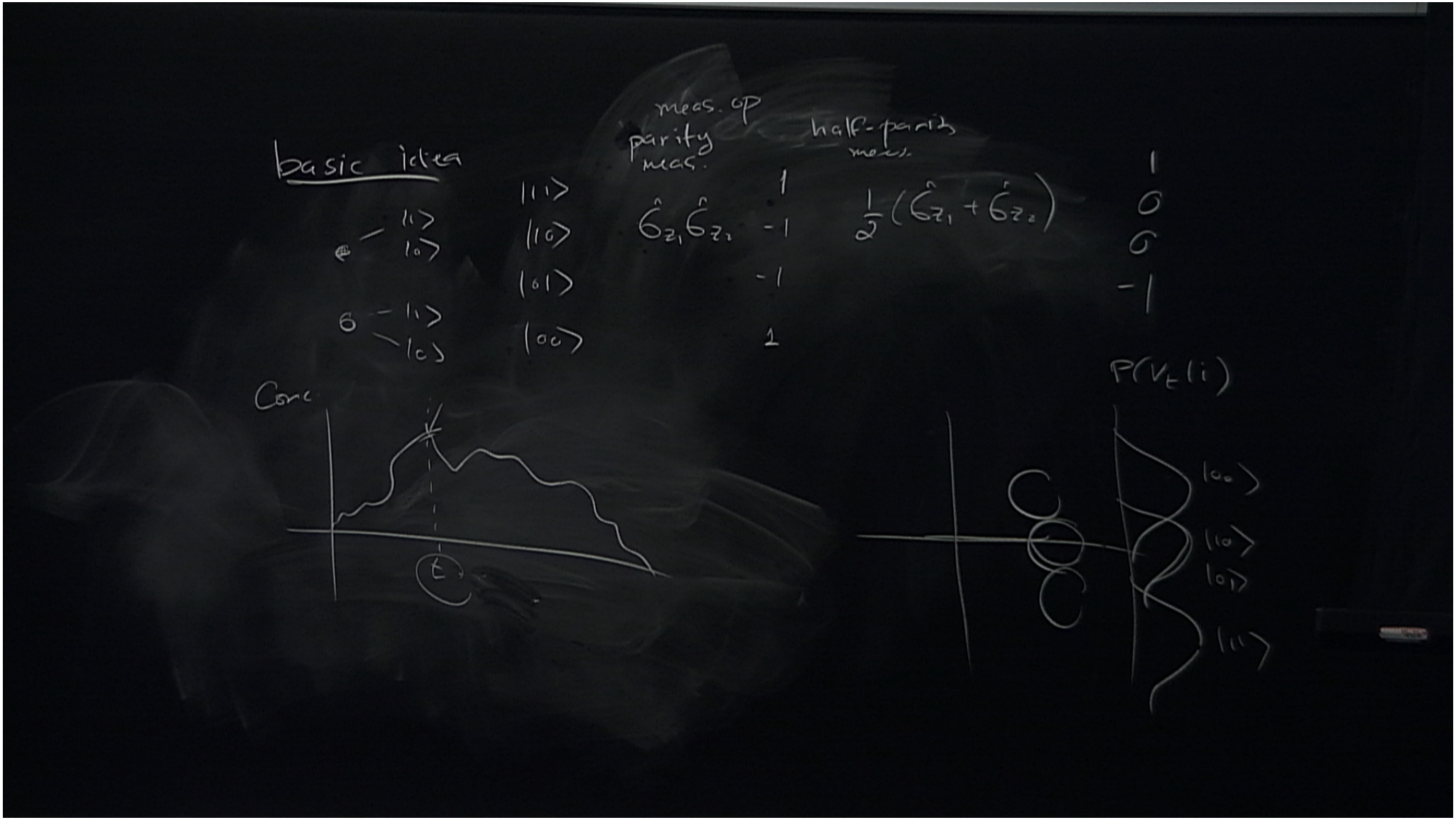
basic idea
meas. op
parity meas.
half-parity meas.
|11>
|10>
|01>
|00>
1
-1
-1
1
1
0
0
-1
Conc
t
P(V_t(i)
|00>
|10>
|01>
|11>

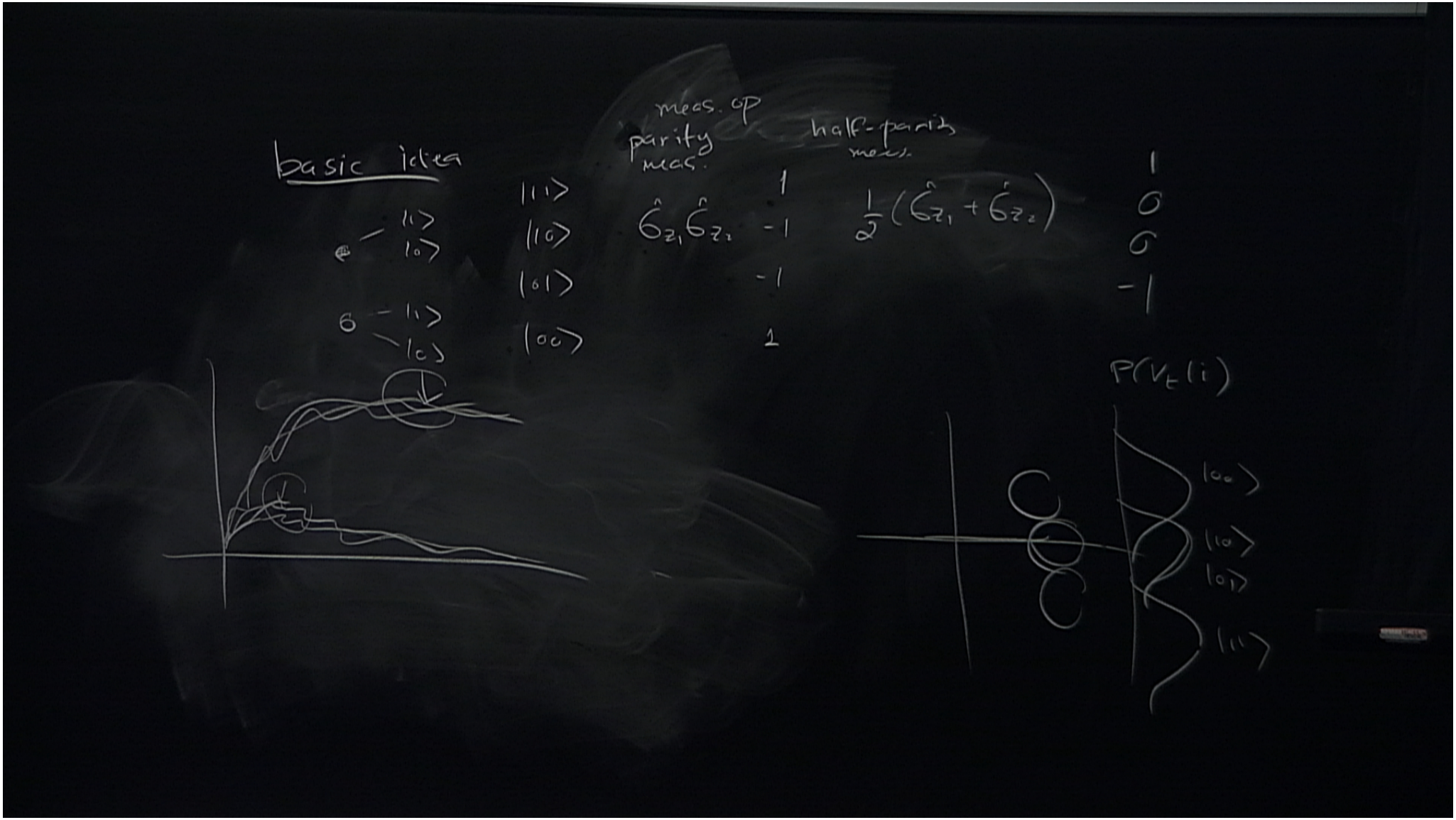
basic idea
meas. op
parity meas.
half-parity meas.
|11>
|10>
|01>
|00>
1
-1
-1
1
1
0
0
-1
P(V_t(i)
|00>
|10>
|01>
|11>